Available online at www.sciencedirect.com
ScienceDirect
Acta Materialia 55 (2007) 5489–5499
Acta MATERIALIA
www.elsevier.com/locate/actamat

Stress generation by shape memory alloy wires embedded in polymer composites

D. Bollas [a,b], P. Pappas [a,c], J. Parthenios [a,b], C. Galiotis [a,b,c,*]

[a] Foundation for Research and Technology Hellas, Institute of Chemical Engineering and High Temperature Chemical Processes, University of Patras, Greece
[b] Inter-Departmental Programme of Graduate Studies in Polymer Science and Technology, University of Patras, Greece
[c] Materials Science Department, University of Patras, Greece

Received 27 February 2007; received in revised form 3 June 2007; accepted 12 June 2007
Available online 9 August 2007

Abstract

Single shape memory alloy (SMA) wires are capable of generating high compressive stresses under constrained conditions when they are thermally activated. In this work, the ability of single SMA wires to act as internal stress generators in fibrous polymer composite systems has been investigated. The stress fields recorded both at the specimen level and internally in the reinforcing fibers by means of Raman microscopy measurements have confirmed that SMA wires can serve as effective stress-actuators. The efficiency of stress generation depends on the wire alloy composition and level of prestrain prior to incorporation into the composite medium. The internal stress distribution in the composite fibers decayed from a position just above the wire surface to the edges of the specimen reaching zero at a distance of approximately 3000 μm. The maximum value of stress recorded in the fibers at a distance of approximately one wire radius was 227 MPa. The significance of these results in the design and operation of adaptive composites systems similar to those examined here is discussed.

Keywords: Polymer matrix composites; Raman spectroscopy; Shape memory alloys (SMAs)

1. Introduction

Shape memory alloys (SMAs) are materials with functional properties associated with the shape memory effect (SME), first observed almost 50 years ago [1]. The SME is based on a reversible transformation between austenitic and martensitic phases of certain alloys which are usually based on Cu, such as Cu–Zn or Cu–Zn–X (where X = Al, Ga, Sn, Si, Ni), and Fe, such as Fe–Pt or Fe–Ni–X (where X = Mn, C) [2]. The most commonly studied and used alloys are those based on Ni–Ti for a variety of reasons, including their larger recoverable deformation, their greater produced work per unit weight and their stable thermomechanical behavior after a long period of reversible activation [2]. The critical temperatures that govern the transformation are denoted as T_{Ms}, T_{Mf}, T_{As} and T_{Af}, where M corresponds to the martensite phase, A to the austenite phase, and s the start and f the finish of each phase formation; it follows that $T_{Mf} < T_{Ms} < T_{As} < T_{Af}$ [2,3].

The incorporation of SMA materials in the form of wires or thin films into host materials, preferably polymers, has been the subject of intense study over the last ten years [4–8]. The resulting hybrid composites belong to the so-called "smart" or "functional" class of materials, since some of their structural properties, such as stiffness, damping capacity or even shape, can be altered by the triggering of the martensite to austenite transformation [4]. It is evident that the performance of these "smart" hybrid systems will depend on the internal stresses generated during SMA activation. For example, certain components can be designed that can undergo large, reversible shape changes

* Corresponding author. Address: Materials Science Department, University of Patras, Greece. Tel.: +30 2610 965 255; fax: +30 2610 965 228.
E-mail addresses: c.galiotis@iceht.forth.gr, galiotis@upatras.gr (C. Galiotis).

1359-6454/$30.00 © 2007 Published by Elsevier Ltd on behalf of Acta Materialia Inc.
doi:10.1016/j.actamat.2007.06.006

as a result of the stresses generated by the embedded SMAs under certain conditions [4].

Since the initial attempts of embedding Nitinol wires into polymers [5,6], much effort (both experimental and analytical) has been made to determine the stress generation at the macroscale and, hence, to assess the capability of the SMA–host medium interface to transmit stress. Most systems examined consisted of an epoxy matrix host in which SMA elements in the form of wires, ribbons or strips have been incorporated. The integrity of the SMA–epoxy resin interface, the integrated SMA displacements, the development of stress contours along the SMA and the host deformation are some of the parameters that have been studied [7–10]. To this end, a variety of experimental techniques has been used, including photoelastic stress analysis [7,8], pull-out tests [7], heterodyne interferometry [8], mechanical tension combined with a thermostatic bath [9] or a CCD camera [10], and digital image correlation [10,11].

More recently SMA elements have been incorporated into polymer composite materials that consist of a matrix resin which is reinforced by commercial fibers such as aramid, carbon or glass. The reason for using a fibrous composite as a host material is the excellent mechanical properties per unit weight that these materials offer, which make them ideal for structural ''adaptive'' or ''smart'' systems [12]. Representative systems studied are beams of epoxy/graphite fibers/SMA wires and epoxy/glass fibers/SMA wires [13,14]. The displacement of similar composite systems during activation was determined by Friend and Morgan [15] using a non-contact optical displacement measuring system and by Doran [16] and Baz et al. [17] using strain gages. Turner's group [18] studied a similar epoxy resin/glass fiber/SMA ribbon system in which they recorded the generated stress as a function of the activation temperature for various prestrain levels, using a Universal Servohydraulic Testing Machine (MTS). Finally, a great deal of data concerning the deformation of an epoxy resin/glass fiber/NiTiCu system as a function of the activation duration, deformation rate and the SMA prestrain level, for different volume fractions of SMA wires, have been generated using TMA [19,20].

The hybrid composites that seem to take precedence over the other systems are those that consist of aramid fibers/NiTiCu wires incorporated into an epoxy resin matrix. These composites incorporate reinforcing fibers and SMA wires of similar Young's moduli (austenite phase) to ensure structural homogeneity [21]; furthermore, the low negative thermal expansion of the aramid fibers leads to the generation of relatively small residual thermal stresses within the composite structure during processing [19]. It is worth mentioning here that an epoxy resin matrix with T_g higher than the activation temperature of the SMA wires must be selected in orer to ensure the generation of recovery stresses within the system [21]. Finally, aramid fibers exhibit a relative high fracture strain, something essential when the ''morphing'' function of an adaptive system is being targeted.

The vast majority of the work done on the determination of the functionality of epoxy resin/aramid fiber/NiTiCu wires systems has taken place within the framework of the ADAPT project [22]. Parlinska et al. [23] determined the generated stresses as a function of activation duration by such a system for various prestrain levels and volume fractions of the wires, using a U-shaped sample holder. Michaud et al. [24] and Balta et al. [25] determined the generated stresses and the resulting deformations with respect to the activation temperature and duration, for a variety of prestrain levels, volume fractions and composite configurations, using a variety of experimental techniques. Similar data concerning various prestrain levels can be found in Refs. [19–21,26,27]. It is worth mentioning here the work of Murusawa et al. [10], in which photoelastic methods are employed to assess the stress distribution within the hybrid composite during the SMA activation. Most of the above works have examined the specimen macroscopic response under wire activation.

Experimental determination of the stress distributions within an epoxy resin/Kevlar 29/NiTiCu wire hybrid system at the microscale, for various wire volume fractions, has been carried out by means of Raman microscopy (RM). This technique employs the reinforcing aramid fibers as stress–strain sensors [28–30] and can map the fiber stresses with a resolution of about 2–3 μm during SMA wire activation. Experimental results in systems incorporating 1, 3, 5, 10 and 20 SMA wires across their wire axis have already been reported [21,31–34].

In the present work an effort is made to assess the capability of SMA wires as stress generators in epoxy resin/aramid fiber composites, not only at the macro- but also at the microscale. In contrast with the results reported previously [33], the experiments are here conducted at fixed strain conditions on an MTS mechanical frame which, in effect, places the whole specimen into tension when compressive stresses are generated during SMA wire activation. The experimental approach involves the mapping of aramid fiber stresses on simple geometries that contain a single SMA wire.

2. Experimental

The capability of single SMA wires to generate compressive stresses, before being incorporated into the composite material, was determined using the recently developed THERMIS system [35]. This consists of a 50 kN Universal Servohydraulic Testing Machine (MTS 858 MiniBionix), a multiple SMA wire activation system, an infrared camera and an analog/digital card able to record the signals of 10 thermocouples. More details on the THERMIS system will be given elsewhere [35].

The specimens consisted of single NiTiCu(6%) and NiTiCu(12%) wires, supplied by @mt, Belgium and Memry Co., USA, respectively. The wire chemical composition and their transformation temperatures are presented in Table 1. All specimens were heated at 100 °C for 10 min

Table 1
Wire chemical composition and transformation temperatures

Cu (% cw)	T_{Ms} (°C)	T_{Mf} (°C)	T_{As} (°C)	T_{Af} (°C)
6[a]	52	37	60	70
12 [36]	47	38	56	64

[a] @mt, Belgium data sheets.

to remove the prestrain caused during packaging. It is worth noting here that the testing of the NiTiCu(12%) wires was done mainly for comparative purposes vis-à-vis previous work [36], while the choice of NiTiCu(6%) was driven mainly by current commercial availability. The 8 cm long SMA wires were gripped on the MTS mechanical frame and then resistively activated by applying a maximum voltage of 2.0 V at a step of 0.2 V per 30 s. The recorded stresses were found to reach a maximum value at 1.8 V. Increasing the applied voltage further did not result in any significant increase in the generated stresses. Since it was not feasible to define precisely the wire temperature inside the composite, an experiment that simulated the wire activation into the composite was conducted for both wires. Each wire was covered by a special thermoresistant sheath filled with a thermoconductive paste. A tiny thermocouple was placed into the sheath to measure the temperature rise during activation. At 2.0 V of maximum applied voltage the measured temperature was 100 and 97 °C for NiTiCu(6%) and NiTiCu(12%) wires, respectively. The sheath covered 1 cm of the wire length and each wire was 300 μm in diameter. During the simulation experiment the samples were protected in a box in order to block possible air streams that may interfere with wire cooling.

The level of voltage supplied to the SMA wires increased up to the point where the maximum stresses were recorded, which in effect is achieved at temperatures greater than T_{Af}. A minimum number of three specimens of (a) as-received SMA wires and (b) wires with 3% prestrain have been tested with the MTS frame. A number of activation cycles were initiated, in order to stabilize the SMA wires.

The hybrid specimens examined here were manufactured in an autoclave by incorporating one as-received NiTiCu(6%) wire, and one 150 μm diameter wire prestrained by 3%. Each wire was placed between two unidirectional prepreg plies of Kevlar 29 fibers embedded into LTM217 epoxy resin. The Kevlar 29 fibers were supplied by Du Pont de Nemours, USA, while the epoxy resin and the prepreg tapes were from ACG, UK. Details of the overall design philosophy and the physical and geometrical characteristics of the adaptive composites, as well as their manufacturing procedure, can be found elsewhere [21,31,32]. It should be mentioned here that the hybrid polymer composites were cured to 70 °C for 12 h and post-cured at 170 °C for 1 h. This ensured that the T_g of the matrix was approximately 160 °C [21], which is well above their activation temperature and the maximum temperature used in the present work.

The macro- and microscale determination of the stress fields developed during the resistive activation ($T > T_{Af}$) of the SMA wires was accomplished by combining the THERMIS System with a remote Raman monitoring system. The MTS was used to record the macroscopic stress field generated by the hybrid specimens, while keeping them under fixed, zero strain. The remote Raman monitoring system designed in house and developed by Jobin Yvon, France was employed to recording the Raman spectra, and hence to determine the stress distribution in the fibers at the microscale. The Raman microprobe uses an optical fiber for Raman light collection, while the laser source has been incorporated into the main body of the microprobe. Detailed description of the remote Raman microprobe will be given elsewhere [37].

A schematic representation of the sampling strategy is presented in Fig. 1a, while a micrograph of part of the cross section of the specimen, whereby aramid fiber Raman spectra were taken, is shown in Fig. 1b. Suitable tabs were attached on the hybrid specimens of dimensions $120.00 \times 13.00 \times 0.25$ mm^3 complying broadly with ASTM D3039/D3039-95a [38]. The specimens were gripped on the MTS at a strain of 0% and a number of activation cycles were initiated, in order to stabilize the SMA wires [36], followed by a steady-state operation. Raman acquisition (30 runs) took place before and after the activation cycles of the SMA wires and also during the steady-state operation. Raman spectra were recorded along fibers parallel to SMA wire direction with a step equal to 30 μm (Fig. 1a). The interrogated fibers were located near the surface of the specimen and at fixed distances from the wire, where tiny thermocouples were placed (Fig. 1a). The sampling locations were determined by an IR camera (Nikon LAIRD 3SH) equipped with a macro lens providing a spatial resolution of 25 μm. Sampling lines on the specimen incorporating the as-received wire were located at 0, −917, 917, −1690, 1690, −3088, 3088, −5883 and 5883 μm from the axis of the SMA wire. The corresponding lines on the specimen incorporating the 3% prestrained wire were located at 0, −568, 568, −732, 732, −1595, 1595, −5660, 5660 μm. The detailed analysis of the Raman spectra elaboration can be found elsewhere [31,32]. The temperature distribution on the specimen surface was recorded by the thermocouples situated exactly at the above locations, while global IR temperature imaging was also undertaken. It should be noted here that the temperature distributions determined by the thermocouples were used to assess the developed stress distributions via RM [28–32]. It is worth adding here that all the activations took place at the same temperature level ($T > T_{Af}$) as this was defined by the thermocouple situated one wire radius above the wire (0 μm distance). All the above measurements took place in an isolated room free from any kind of air streams and under a constant room temperature of 25 °C.

For better understanding of the results presented here, it should be noted that the specimens imposed a compressive force on the mechanical frame (MTS) during resistive thermal activation, since they were kept under "fixed-strain"

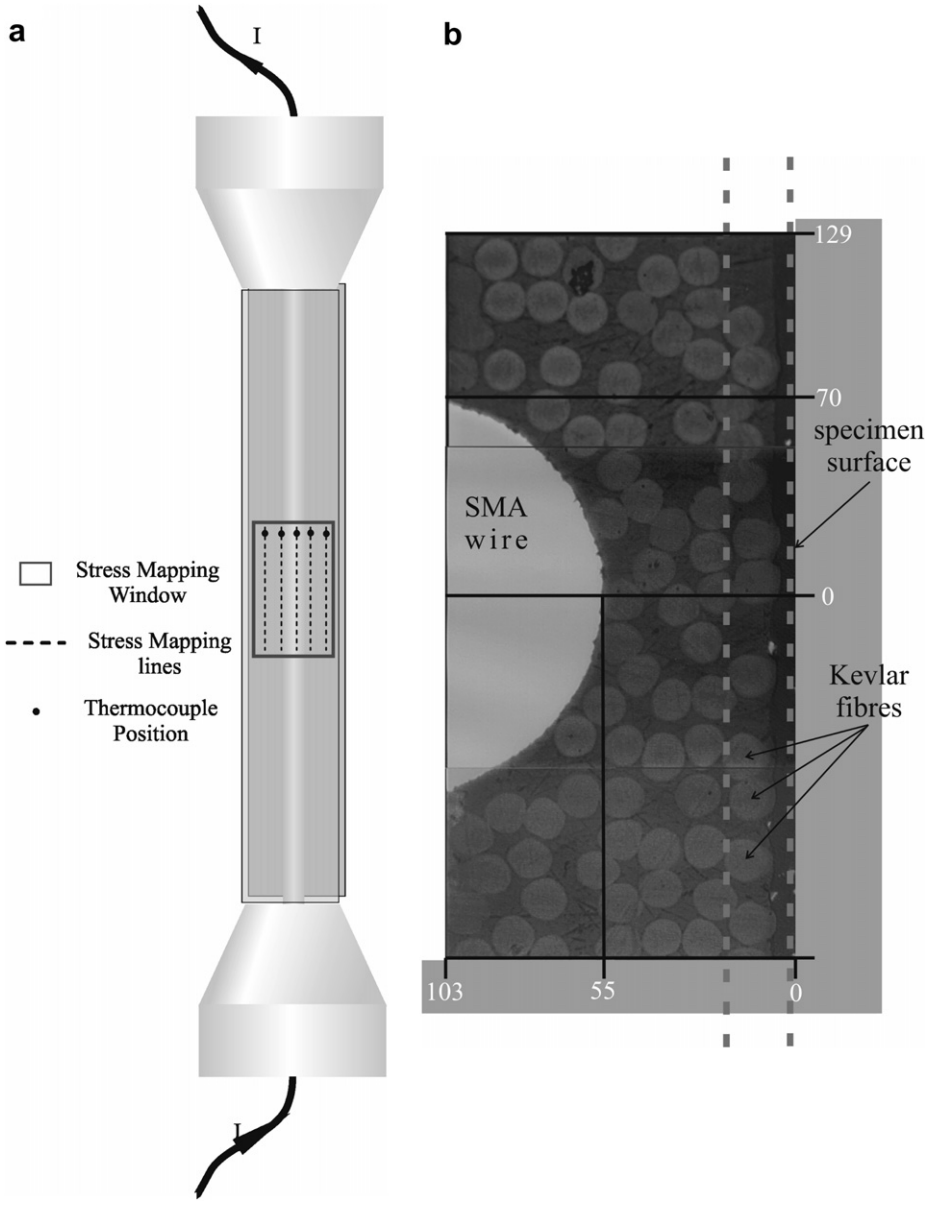

Fig. 1. (a) Schematic representation of an SMA composite specimen and the Raman sampling line, and (b) a microphotograph of a portion of the cross-section. A part of the Raman sampling region on the specimen surface is defined by the dashed lines. All distances in (b) are measured in μm.

conditions, whereas the specimen is experiencing tension. In other words, since the wire wants to contract, and is prevented both by the surrounding matrix and the fixed grip condition (zero global strain), then a tensile stress gradient is developed which is transferred to the Kevlar fibers by matrix shearing. This effect is identical to the stress perturbation observed adjacent to a single fiber fracture in full composites containing parallel fibers. It is worth adding here that the measurements are conducted at the middle of the specimen to avoid any effect that the grips may have on the local stress development.

Finally, for comparative purposes, plain, unconstrained composite samples were tested at elevated temperatures (60, 80 and 100 °C) in order to define the developed thermal stresses. The geometric dimensions of the samples examined were identical with those hybrid samples used in the present study and prepared with the same curing procedure described previously. The thermal stresses were measured by recording 200 Raman spectra randomly from fibers located at the surface of the sample. By applying a statistical methodology described in detail in Ref. [31], the thermal stress distribution at elevated temperatures was determined. The above measurements took place in an isolated room free from any kind of air streams.

3. Results

3.1. Activation of single NiTiCu wires in the air

Fig. 2 shows the MTS recorded stresses as a function of activation time obtained from a single as-received NiTiCu(6%) wire and from a wire of the same alloy

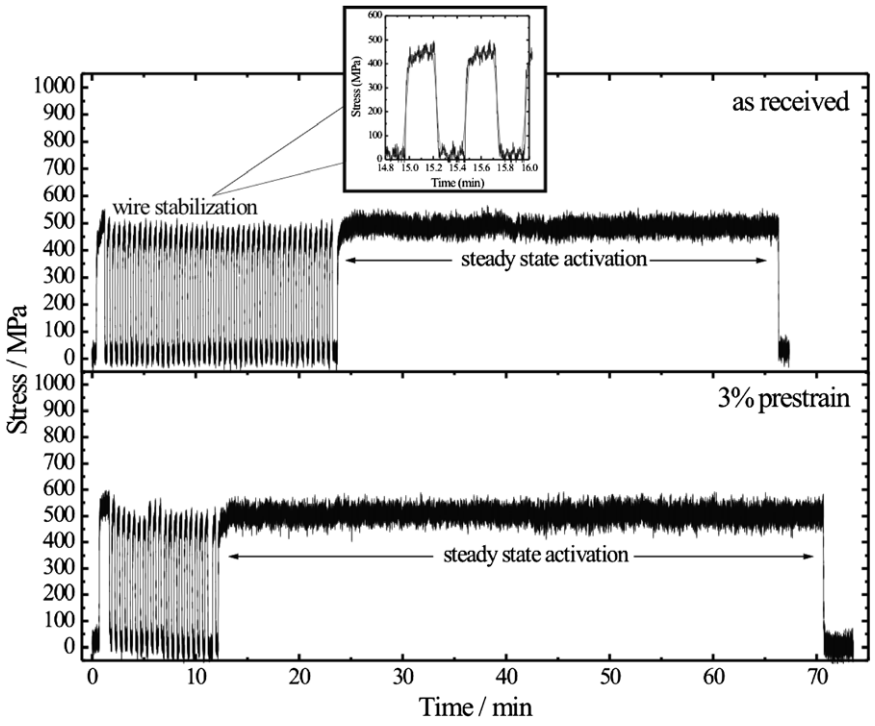

Fig. 2. Generated stresses from an as-received single NiTiCu(6%) wire and a single NiTiCu(6%) with 3% prestrain.

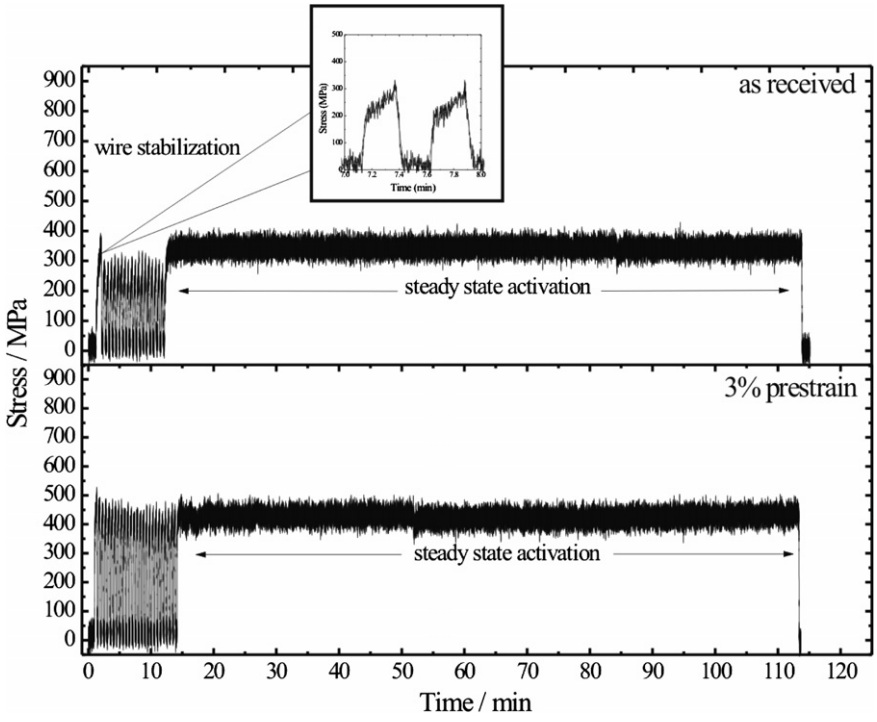

Fig. 3. Generated stresses from an as-received single NiTiCu(12%) wire and a single NiTiCu(12%) with 3% prestrain.

composition prestrained by 3% in air. For the as-received wire, values of recovery stresses up to 500 MPa are recorded both during stabilization and steady-state activation. In the case of the prestrained wire, maximum recovery stresses up to 550 MPa are generated. The corresponding results for the as-received and that with 3% prestrained NiTiCu(12%) wires are presented in Fig. 3. In this case, the as-received SMA wire is capable of generating constant stresses up to approximately 350 MPa, while the generated stress from the prestrained NiTiCu(12%) wire remains

constant at almost 450 MPa. The fluctuation width of generated stress values of approximately 50 MPa was due to the sensitivity of the 2.5 kN load cell that was used at its 10% dynamic range.

3.2. Pure K29/epoxy composite at elevated temperatures

The residual and thermal stresses developed in pure K29/epoxy composites at elevated temperatures are shown in Fig. 4, where a linear dependence of thermal stresses on temperature can be seen. The x-axis of the diagram in Fig. 4 corresponds to the temperature difference from the ambient value of 25 °C. The development of thermal stresses should be taken into account when the stresses generated by the SMA wires embedded in the composites are calculated. These results reveal that the CTE (thermal expansion coefficient) of the pure K29/epoxy composites is positive, giving rise to tensile thermal stresses in the composite specimen. A detailed description of the experimental procedure employed to obtain the above results will be given elsewhere [41].

3.3. Activation of NiTiCu(6%) wires embedded in K29/epoxy composites

3.3.1. Composite system incorporating single as-received wire

In Fig. 5 the steady-state temperature distribution developed within the K29/epoxy/[as-received NiTiCu(6%) wire] during steady-state wire activation as a function of the distance from the wire is presented. As is evident, the temperature distribution has a maximum just above the wire surface and then decays towards the specimen edges (Fig. 1). The agreement between the values recorded by the attached thermocouples and those obtained by the IR camera is satisfactory bearing in mind the sampling differences of the two techniques. The maximum deviation is observed at the wire location and is of the order of 14 °C (Fig. 5). Relatively large differences are also observed near the specimen edges, the origin of which will be discussed later.

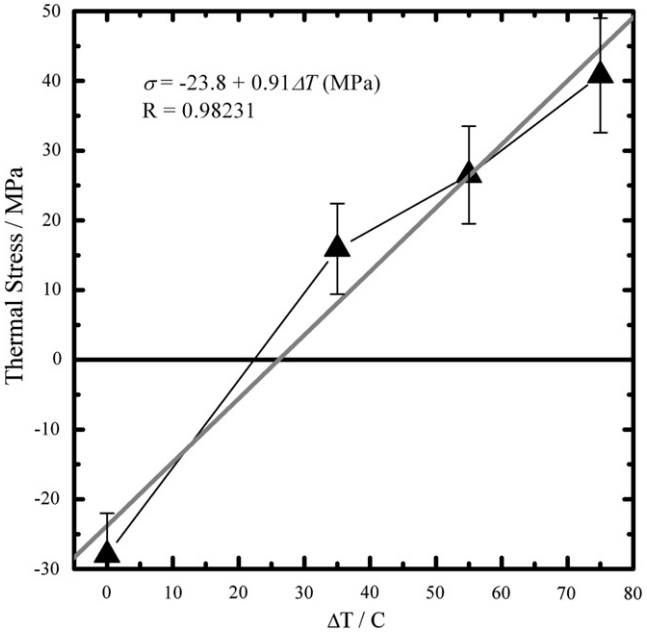

Fig. 4. Thermal stresses as a function of temperature for a pure aramid fibre/epoxy composite. The X-axis corresponds to the difference of the applied temperature from the ambient one. The data point at $\Delta T = 0$ °C corresponds to the residual stresses developed during the composite fabrication procedure.

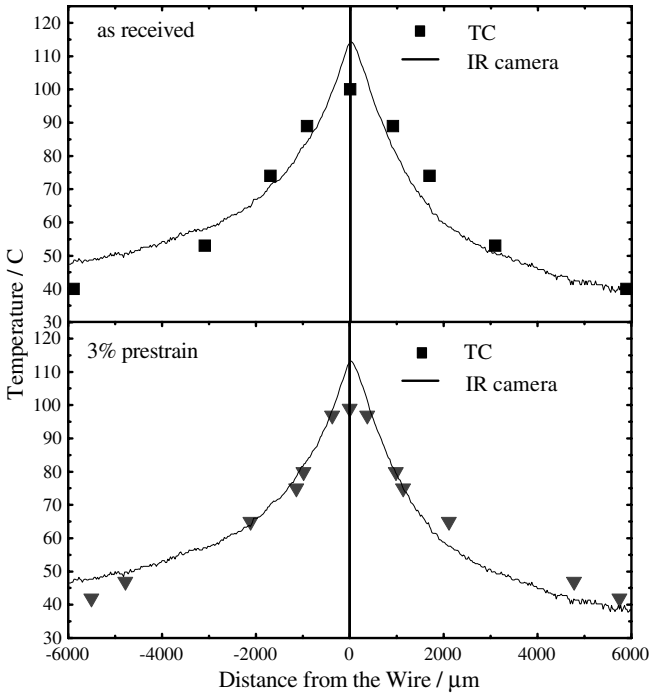

Fig. 5. Temperature distribution of SMA composite specimens incorporating a single as-received and a 3% prestrained NiTiCu(6%) wire. The accuracy of thermocouple measurements was 2–3 °C.

Taking into account the temperature distribution that develops within the K29/epoxy/SMA wire composite during steady-state activation, the distribution of the developed thermal stresses can be calculated. The calculation was based on the linear relationship of thermal stresses, σ_{thermal}, with temperature according to the formula:

$$\sigma_{\text{thermal}} = -23.8 + 0.9\Delta\text{T (MPa)}, \quad (1)$$

where $\Delta T = T - T_0$, and T_0 is the ambient temperature (25 °C). All temperature values, T, correspond to those obtained by thermocouples and are given in Fig. 5. The results of the above calculation are presented in Fig. 6. The thermal stresses are greatest above the location of the wire, where a mean value of approximately 45 MPa has been calculated, and decrease with distance from the wire. At a distance of approximately 3000 μm the thermal stresses become equal to the residual stresses in the fibers.

The MTS-recorded stresses generated by the SMA composite during steady-state wire activation as a function of time are shown in Fig. 7. During activation, the SMA

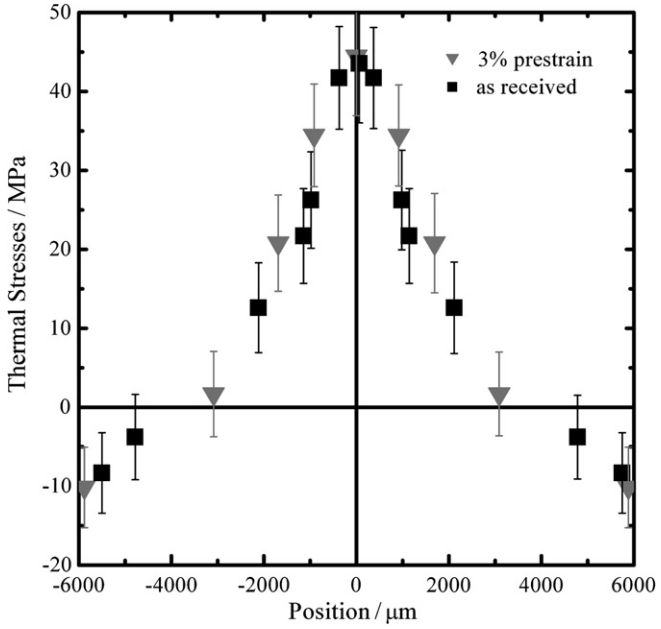

Fig. 6. Thermal stress distribution in SMA composite specimens incorporating a single as-received and a 3% prestrained SMA NiTiCu(6%) wire.

composite was capable of generating stresses of about 4 MPa that appear to be quite stable within the timeframe examined here.

A brief explanation of the methodology used to extract the values of stress generated by the SMA wire is given here. The 1611 cm^{-1} Raman band of the aramid fiber [31] was chosen as the spectroscopic sensor due to its high stress sensitivity. In order to evaluate the fiber stress distribution prior to SMA wire activation, all 270 spectra collected from the Raman mapping lines (Fig. 1) were statistically analyzed. The peak values were represented by a normal distribution with a maximum probability density value at $v_0 = 1611.18 \pm 0.02$ cm^{-1} for all specimens used in this work. The mean peak position of the 1611 cm^{-1} band taken from prepreg fibers prior to specimen fabrication were found to be $v_r = 1611.09 \pm 0.01$ cm^{-1}. Detailed description of the above statistical procedure can be found elsewhere [31].

Using the established relationship between Raman shift, Δv_{mech}, and axial stress, σ (in GPa) [30,31]:

$$\Delta v_{mech} = (v_0 - v_r) = -4\sigma \ (cm^{-1}), \quad (2)$$

the mean value of the residual stresses was found to be −22.5 MPa. As confirmed earlier [30], the above relationship (2) is valid for any temperature T. Let v_r be the mean peak position of the 1611 cm^{-1} Raman band at temperature T. For any stress σ, the Raman band positions will be shifted to lower values according to [30]:

$$\Delta v_r = -0.015(T - T_0) \ (cm^{-1}). \quad (3)$$

In addition to the effect of stress and temperature on the wavenumber position, it is also necessary to estimate the effect of developing thermal stresses (Fig. 6) at elevated

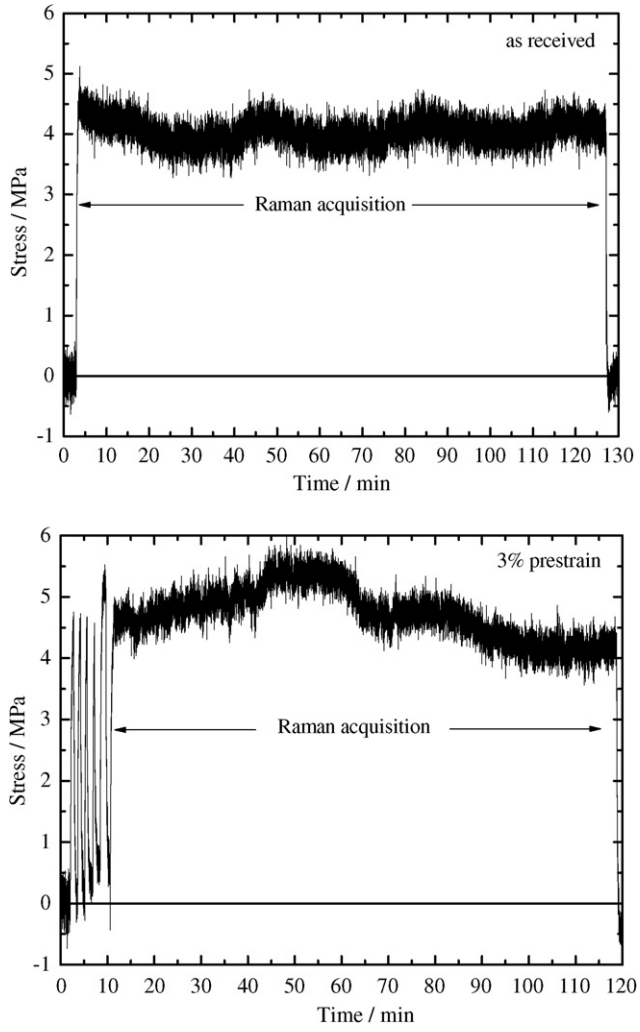

Fig. 7. Generated stresses from SMA composite specimens incorporating a single as-received and a 3% prestrained NiTiCu(6%) wire.

temperature on the Δv. Hence, by combining Eqs. (1) and (2), the contribution of thermal stresses to the shift in v_0 can be found by:

$$\Delta v_{thermal} = -0.004(T - T_0) \ (cm^{-1}). \quad (4)$$

Thus the overall shift Δv_{total} during SMA wire activation should be estimated by:

$$\Delta v_{total} = (v_T - v_r) = \Delta v_{SMA} = \Delta v_{thermal} = \Delta vT, \quad (5)$$

where v_r is the peak position of the 1611 cm^{-1} band at temperature T and Δv_{SMA} is the pure contribution to the shift in v_r caused by mechanical stress from the activated SMA wire.

Substituting the Eqs. (2)–(4) into (5), the stress generated by the SMA wires and transmitted to the aramid fibers (Fig. 8a) is given by:

$$\sigma_{SMA} = -\frac{\Delta v_{total} = 0.019(T - T_0)}{4} \ (GPa). \quad (6)$$

It is worth noting that the stresses as a function of the position (Fig. 8b) on the completion of the SMA cycle were evaluated from Eq. (2), since the specimen is at room

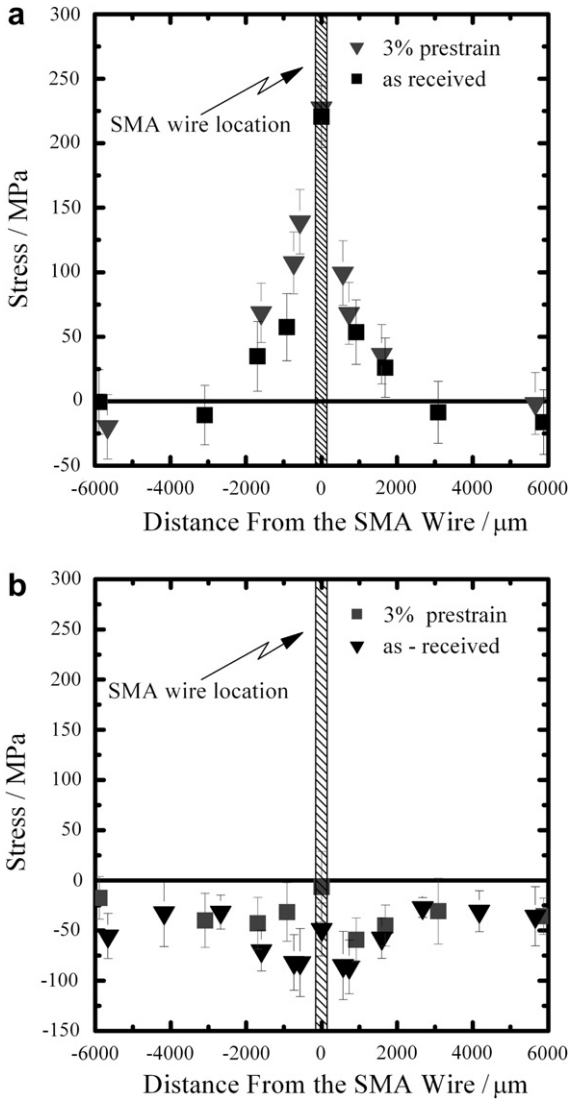

Fig. 8. The distribution of transmitted fibre stresses of SMA composite specimens incorporating a single as-received and a 3% prestrained NiTiCu(6%) SMA wire (a) during and (b) after steady-state activation of the wire.

temperature, T_0. It must be noted that the specimens were cooled for a long time after the SMA activation to ensure that thermal equilibrium has been reached.

The stresses generated purely by the SMA wire and transmitted to the aramid fibers are greatest above the location of the wire (position 0 μm), where a mean value of 200 MPa was calculated (Fig. 8a). The stress decays with distance from the wire, reaching zero at a distance of approximately ±3000 μm. The overall residual stress field developed within the composite on the completion of steady-state activation (Fig. 8b) appears to be compressive with a mean value equal to approximately −25 MPa at distances far from the wire (>3000 μm), which corresponds to the initial level of residual stress developed during specimen fabrication. It is interesting to note that right above the wire the stress is zero, and then it becomes compressive with maximum values equal to −50 MPa; finally, the stress approaches a constant value of −25 MPa over almost the whole width of the specimen.

3.3.2. Composite system incorporating the 3% prestrained wire

Fig. 5 shows the temperature distribution of the thermal field transmitted to the aramid fibers (IR and the thermocouple measurements) by the resistive heating of the embedded 3% prestrained SMA wire, as a function of distance. As with the stress measurements, the maximum temperature is recorded right above the wire surface; this then decay towards the edges of the specimen (Fig. 1). The agreement between the two sets of measurements is again satisfactory. Nevertheless, certain discrepancies at the two extremes of the distribution (above the wire and at the specimen edges) are observed. The thermal stress distribution that results from the corresponding temperature distribution (Fig. 5) is shown in Fig. 6.

The MTS-recorded stresses generated by the SMA composite during steady-state wire activation as a function of time are shown in Fig. 7. During activation, the SMA composite was capable of generating stresses of about 5 MPa that appear to be quite stable within the timeframe examined here.

The stresses generated purely by the SMA wire and transmitted to the aramid fibers are greatest above the location of the wire (position 0 μm), where a mean value of 227 MPa was calculated (Fig. 8a). The two regions on either side of the wire appear to be asymmetric; on the left side the generated stress field decays, reaching zero at a distance of about 4000 μm, whereas on the right side the stress decay is steeper and reaches zero at about 3000 μm. The overall residual stress field developed within the composite on the completion of the steady-state activation (Fig. 8b) appears to be compressive with a mean value equal to approximately −25 MPa at distances far from the wire location (>3000 μm), which corresponds to the initial level of residual stresses developed during specimen fabrication. It is interesting to note that right above the wire the stress is zero, then becomes compressive with maximum values equal to −75 MPa, and decays towards a constant value of −25 MPa at 3000 μm on either side of the specimen. In qualitative terms the shape of the stress distribution is the mirror image of that obtained during the wire activation (Fig. 8a), which demonstrates a reversal of the stress field on the completion of the experiment. As argued later, it appears that the effective permanent tensile deformation of the wire during steady-state activation in its "austenite" phase results in the generation of compressive stresses on cooling as the mechanical frame is kept under a "fixed-grip" condition.

4. Discussion

4.1. Generated stresses by single NiTiCu wires in the air

The generated stresses in an as-received and a 3% prestrained NiTiCu(6%) wire are shown in Fig. 2. Regardless

of prestrain level, the generated maximum stress of approximately 500 MP, remains exceptionally steady under steady-state operation. This behavior is not as yet fully understood. One likely explanation is that these wires were prestrained to their maximum level by the manufacturers themselves. This is also corroborated by the fact that a training process is required to set a new memory and alter the transformation characteristics of the wires in order for the prestrain level to have a significant effect on the generated mechanical stress level [35].

Regarding the NiTiCu(12%) wire (Fig. 3), the results are similar to those of the NiTiCu(6%) wire reported above; the as-received wire (Fig. 3) is capable of producing maximum stresses of 350 MPa, while stresses up to 450 MPa are produce by the equivalent wire prestrained prior to the test (Fig. 3). It should be mentioned here that the latter values are in good agreement with those reported in the literature [36]. The fact that again even the as-received wire is generating stresses could be attributed to one of the two reasons mentioned above, while it should be noted here that the same phenomenon has been recorded during tests on 300 μm diameter NiTi wires obtained also from @mt, Belgium [35]. The stress-generating capability of just the NiTiCu(12%) wires from this company has been tested previously [19–21,26,27] using a tensile machine equipped with an oil bath. The possibility that the present wires exhibit a two-way SME behavior can be ruled out as such wires are not capable of generating high stresses under constrained conditions [2] .

It is worth mentioning here that the stresses produced by the as-received NiTiCu(12%) wire are now considerably smaller than those produced by the prestrained equivalent. Since the two types of wires originate from different manufacturers, it is of no surprise that they differ as far as their original prestrain level is concerned. Finally, the small differences of maximum generated stresses observed between NiTiCu(12%) and NiTiCu(6%) wires reflect dissimilarities in their transformation paths [39]. Overall, it is expected that both types of wires should be capable of generating stresses of similar magnitude when embedded in composites.

4.2. Generated stresses by a NiTiCu(6%) wire embedded in K29/epoxy composites

4.2.1. As-received wire

Prior to the determination of the stress distribution both at macroscale (THERMIS system) and the microscale (aramid fibers), it is important to assess the temperature profile within the same area of measurement. As shown in Fig. 5, the resulting distribution has a maximum of 110 °C above the wire and decays away to about 40–45 °C at a distance of 6000 μm (specimen edges). This kind of distribution obtained from an IR camera or by attaching thermocouples across the specimen is very important since it contributes to the formation of the resulting stress distribution at the microscale. In addition, it can be used for calculating the thermal stress distribution (Fig. 6). Since aramid fibers have a negative axial thermal expansion coefficient, it is evident that the high temperatures near the wire plus the high compressive fields generated by the wire transformation will induce a non-uniform stress field in the case of a single wire composite specimen examined here. To start with, during steady-state activation, the large compressive field generated by the wire and up to a distance of about 1000 μm on either side (Fig. 8a) is translated into a machine tensile stress (fixed grip condition) that gives rise to tensile stresses in the fibers up to a maximum 200 MPa just above the location of the wire.

Upon activation of the as-received NiTiCu(6%) wire, the composite specimen generates constant compressive stress which, under constrained conditions, is translated into tensile MTS stress (Fig. 7). Again the generated maximum stress remains steady under steady-state operation, which indicates no deterioration of the wire/epoxy/aramid interface within the times involved in the experiment (Fig. 7).

The origin of the permanent high compressive values in the fibers in the region of ±3000 μm recorded after reversing to martensite, shown in Fig. 8b, can be explained as follows: when the wire is embedded into a composite the imposed constrained conditions, both longitudinally (by the MTS) and laterally (by the composite material), result in the generation of tensile forces which are counterbalanced by the compression of the specimen by the mechanical assembly (“fixed-strain” condition).

4.2.2. 3% prestrain wire

The results of the temperature distribution shown in Fig. 5 are similar to those obtained for the as-received wire. The resulting distribution has a maximum of 120 °C above the wire and decays away to about 35–40 °C at a distance of 6000 μm (specimen edges). Once more there is a good agreement between the distributions obtained by the two techniques and any discrepancies are attributed mainly to sampling differences. The largest discrepancy is observed right above the wire surface, which is probably due to changes in emissivity which may alter the obtained IR profile. In general the thermocouple data are considered more accurate as they are taken near the plane of aramid fibers interrogated by RM, whereas the IR data have also a depth component. Finally, the asymmetry of the IR temperature distribution, which leads to large discrepancies between IR and thermocouple values on the right-hand side of the distribution, indicates that the camera was not placed exactly perpendicularly to the specimen surface and/or there was some specimen twisting during activation.

The generated maximum stress, Fig. 7, is higher than in the case of the as-received wire which confirms that the higher the prestrain, the greater the stress generated. Since both wires in the air under constrained conditions generate approximately the same amount of stress, the differences in the stress generation and subsequent stress transmission to the aramid fibers of the composite must be due to differences encountered at the interface between the two

specimens. Indeed, differences in the wire lateral contraction (not examined) here between the two specimens may be responsible for the relatively weaker stress transmission in the case of the composite sample containing the as-received wire. Previous work by others [20,21,26,27,40] has confirmed the importance of the strength of the wire–epoxy interface in stress transmission.

Regarding the stress distribution prior to activation, the residual stress field in the aramid fibers fluctuates around a relatively small compressive stress of about −22.5 MPa. However, during steady-state activation, the large compressive field generated by the wire, and up to a distance of approximately 3000 μm on either side of the wire, is translated into a machine tensile stress (fixed grip condition) that gives rise to tensile stresses in the fibers of up to 227 MPa just above the location of the wire. Finally, it is interesting to note that reversing to martensite, as is evident from Fig. 8b, causes the wire to again come under compression by the mechanical frame and the whole distribution is now reversed, as discussed previously.

5. Conclusions

The ability of a single NiTiCu(6%) wire to act as an internal stress generator in a hybrid system has been investigated, both at the macro- and the microscale. Testing a single wire of this type showed that it is able to produce a significant amount of compressive stress while being activated, regardless of its prestrain level. This leads to the assumption that the initial prestrain induced during manufacturing is sufficient for stress generation under constrained conditions. The NiTiCu(12%) single wire, examined for comparison, also exhibits a similar ''behavior'' but it was found to be less efficient than the NiTiCu(6%) wire.

The macroscopic stress fields produced by two hybrid specimens, incorporating an as-received and a 3% prestrained NiTiCu(6%) wire, during stress activation, has been recorded. Results indicate that the 3% prestrained wire is more efficient in transmitting the stresses that are generated to the system, probably due to the formation of a wire/matrix interface of higher strength than the corresponding interface of the as-received wire. This fact has been also confirmed through the stress state investigation of the system via RM. The form of the internal stress distribution seems to decay from a position right above the wire surface to the specimen edges, reaching zero at a distance of approximately 3000 μm. Furthermore, the axial constraining of the wire by the epoxy resin, which prevents the former from relaxing during cooling, results in the formation of an internal stress distribution within the specimen on the completion of the activation cycle.

Acknowledgements

The authors acknowledge the General Secretariat of Research and Technology, Ministry of Development, Hellas for funding Mr. Bollas and Mr. Pappas and finally the Nanofun-Poly Network of Excellence of the European Communities for supporting the Research Group.

References

[1] Chang LC, Read TA. Trans AIME 1951;189:51.
[2] Duering TW, Melton KN, Stöckel D, Wayman CM. Engineering aspects of shape memory alloys. 1st ed. London: Butterworth-Heinemann; 1990.
[3] Otsuka K, Wayman MC. Shape memory materials. 1st ed. Cambridge: Cambridge University Press; 1998.
[4] Gandhi MV, Thompson BS. Smart materials and structures. 1st ed. London: Chapman and Hall; 1992.
[5] Liang C, Jia J, Rogers C. Behavior of shape memory alloy reinforced composite plates, Part II: results. In: Proceedings of the 30th Structures, structural dynamics and materials conference, AIAA-89-1331-CP; 1989. p. 1504.
[6] Rogers CA. J Acoust Soc Am 1990;88(6):2803–11.
[7] Jonnalagadda KD, Kline GE, Sottos NR. Exp Mech 1997;37(1):78.
[8] Jonnalagadda KD, Sottos NR, Qidwai MA, Lagoudas DC. J Intell Mater Syst Struct 1998;9(5):379.
[9] Yamashita K, Shimamoto A. Key Eng Mater 2004;270–273:2179.
[10] Murusawa G, Yoneyama S, Tohgo K, Takashi M. Key Eng Mater 2004;270–273:2172.
[11] Umezaki E, Ichikawa T. Int J Mod Phys B 2003;17(8&9):1750–5.
[12] Hull D, Clyne TW. An introduction to composite materials. 2nd ed. Cambridge: Cambridge University Press; 1996.
[13] Hebda DA, Whitlock ME, Ditman JB, White SR. J Intell Mater Syst Struct 1995;6:220.
[14] Xu Y, Otsuka K, Yoshida H, Nagai H, Kishi T. Smart Mater Struct 2004;13:196.
[15] Friend CM, Morgan NB. J Phys IV 1995;5:1171.
[16] Doran CJ. The effect of prestrain on the actuation performance of embedded shape memory alloy wires. In: Proceedings of the second European conference on smart structure and materials, Glasgow; 1994.
[17] Baz A, Chen T, Ro J. Composites: Part B 2000;31:631.
[18] Turner TL. Thermomechanical response of shape memory alloy hybrid composites. PhD thesis. National Aeronautics and Space Administration, Langley Research Center, Hampton, VA, USA.
[19] Zheng YJ, Schrooten J, Tsoi KA, Sittner P. Soc For Exp Mech 2003;43(2):194.
[20] Zheng YJ, Cui LS, Schrooten J. Mater Sci Eng A 2005;390:139.
[21] Schrooten J, Michaud V, Parthenios J, Psarras GC, Galiotis C, Gotthard R, et al. Mater Trans 2002;43(5):961.
[22] ADAPT final report. Project number BE97-4134, funded by the European Community under the Industrial and Materials Technologies Programme (Brite-EuRam III); 2001.
[23] Parlinska M, Clech H, Balta JA, Michaud V, Bidaux J-E, Manson J-AE, et al. J Phys IV France 2001;11:197.
[24] Michaud V. Scripta Mater 2004;50:249.
[25] Balta JA, Michaud VJ, Parlinska M, Gotthard R, Mänson J-AE. Adaptive composite materials processing. In: Cunha AM, editor. Proceedings of the European conference on macromolecular physics, structure development upon polymer processing: physical aspects, Guimaraes, Portugal, 24–28 September, 2000, vol. 24I. European Physical Society; 2000. p. 33.
[26] Tsoi KA, Schrooten J, Zheng Y, Stalmans R. Mater Sci Eng 2004;A368:299.
[27] Zheng YJ, Schrooten J, Cui LS. Intermetallics 2005;13:305.
[28] Galiotis C, Parthenios J. In: Gregoriou VG, Braiman MS, editors. Vibrational spectroscopy of biological and polymeric materials. London: Taylor & Francis; 2006. p. 35–98 [chapter 2].
[29] Psarras GC, Parthenios J, Bollas D, Galiotis C. Chem Phys Lett 2003;367/3-4:270.

[30] Bollas D, Parthenios J, Galiotis C. Phys Rev B 2006;73(9). Art. No. 094103.
[31] Psarras GC, Parthenios J, Galiotis C. J Mater Sci 2001;36:535.
[32] Parthenios J, Psarras GC, Galiotis C. Comp A: Appl Sci Manuf. 2001;32:1735.
[33] Bollas D, Koimtzoglou C, Anagnostopoulos G, Psarras GC, Parthenios J, Galiotis C. A new approach for assessing the interface efficiency on standard full-composite specimens. In: Proceedings of the 10th European conference on composite materials, Brugge, Belgium; 2002.
[34] Bollas D, Parthenios J, Galiotis C. Non-destructive study of thermal dissipation in shape memory alloy hybrid composite systems. In: Proceedings of the 11th European conference on composite materials, Rhodes, Greece; 2004.
[35] Pappas P, Bollas D, Parthenios J, Drakopoulos V, Galiotis C. Smart materials and structures. 2007 [accepted for publication].
[36] Tsoi KA, Schrooten J, Stalmans R. Mater Sci Eng 2004;A368:286.
[37] Parthenios J, et al. J Raman Spectrosc [submitted for publication].
[38] ASTM D3039/D3039-95a. Standard test method for tensile properties of polymer matrix composite materials.
[39] Nam TH, Saburi T, Shimizu K. Mater Trans JIM 1990;31(11): 959.
[40] Tsoi KA, Stalmans R, Schrooten J. Acta Mater 2002;50:3535.
[41] Anagnostopoulos G, Parthenios J, Galiotis C. Mater Lett [in press].